Performance of Channel Coding and Equalization for Acoustic Telemetry Along Drill Strings

Konstantinos Pelekanakis and Mandar Chitre
Acoustic Research Laboratory
National University of Singapore
Singapore, 119223

Lakshmi Sutha Kumar and Yong Liang Guan
School of Electrical and Electronic Engineering
Nanyang Technological University
Singapore, 639798

***Abstract*—Real-time telemetry during drilling thousands of meters below the surface plays a key role in efficient utilization of oilfields. Current mud-pulse commercial systems are limited to only a few bits per second (bps). In this paper, we are interested in acoustic data transmission through the steel body of the drill string. We propose trellis coded modulation (TCM) coupled with multicarrier modulation. To cope with the intersymbol interference (ISI) and any synchronization issues at the receiver, joint carrier-phase synchronization and decision feedback equalization is used. In addition, weights based on the knowledge of the signal-to-noise-ratio (SNR) at different passbands are incorporated into the modified Viterbi decoder to improve the bit-error rate (BER). By using a realistic model of a 1-km-drill string channel, the BER performance of the acoustic system is demonstrated while achieving a signaling rate of 400 bps, about two orders of magnitude higher than current state-of-art mud-pulse telemetry systems. In addition, our results demonstrate that the decision feedback equalizer (DFE) is vastly less power-hungry than orthogonal frequency division multiplexing (OFDM).**

I. Introduction

Logging while drilling (LWD), i.e., transmission of down-hole data (temperature, pressure, drilling direction, to name a few) to the surface rig increases the likelihood of finding oil reserves and improves well stability. Telemetry systems achieving data rates of hundreds of bits per second (bps) over very long drill strings (e.g., 8 km) would have a huge economic impact in the oil and gas industry since many drilling operations rely on the availability of real-time data about the wellbore condition [1]. Mud-pulse telemetry, the most widely used technique today, exhibits a very low transmission rate (up to 10 bps) due to low carrier frequencies [2]. Wireline systems are inefficient in terms of cost and maintenance [3]. Electromagnetic waves suffer from high attenuation caused by the formation conductivity and so they have limited usage [4]. Since the early 1970s, the industry has also focused on understanding acoustic wave propagation along the steel body of the drill string due to the broadband nature of the acoustic drill string channel [5].

The challenges associated with acoustic telemetry are multipath propagation leading to passbands and stopbands, attenuation and non-stationary noise. The confluence of all these effects often results in low signal-to-noise ratio (SNR) at the receiver. According to [6], rates of hundreds of bps could be potentially achieved over a 2-km-drill string. Yet, studies that propose bandwidth-efficient acoustic communications are scarce. The available published results rely on orthogonal frequency division multiplexing (OFDM) modulation as a practical phase-coherent telemetry system due to its ability to cope with the drill string's extended multipath. Probably the first feasibility test of an OFDM system was conducted by Memarzadeh [6]. In that work, the author managed to achieve 30 bps over a $3700\,\mathrm{ft}$ drill string channel. A major limitation of that system was the carrier-phase rotation due to lack of receiver synchronization. Gao et al. [7] demonstrated that an OFDM system could potentially achieve hundreds of bps through a $6000\,\mathrm{ft}$ drill string, yet, the design of this system was not published. The authors in [8] presented a high-rate OFDM system for a 55-m-drill string. A notable characteristic is that error correction codes were not tested because the additive noise was not significant in that system.

This paper represents the first attempt to deal with the drill string's extended echoes using time-domain equalization. The proposed system combines trellis coded modulation (TCM) with multicarrier modulation at the transmitter. The transmitted waveform consists of signals of different bandwidths and carrier frequencies enabling transmission over different passbands. Decision feedback equalization coupled with carrier-phase synchronization is used to cope with multipath within each passband [9]. In addition, reliability weights are used in the Viterbi decoder according to the SNR of each passband in order to reduce the BER of the system. System performance is analyzed by using a realistic channel model of 1-km-drill string.

II. The drill string acoustic channel

A typical drill string is a periodic steel structure consisting of hollow pipes (roughly $10\,\mathrm{m}$ long with diameter of $125\,\mathrm{mm}$) connected together by heavy threaded tool joints (collars) [1]. To assess the effectiveness of an acoustic communication system, one needs to know the operational frequency bands. Several studies have reported drill string responses in the frequency band 0-2 kHz [1], [7], [10]. A notable characteristic of the drill string acoustic channel is the presence of passbands and stopbands, as shown in Figure 1(a). This comb-like structure of the acoustic channel is due to the fact that at each joint-pipe junction, the acoustic pulse is partially reflected, leading to a complicated set of constructive/destructive interference pulses at the other end. These multiple reflections result in a signal delay spread in the order of hundreds of ms. The positions of pass bands and stop bands are dictated by the

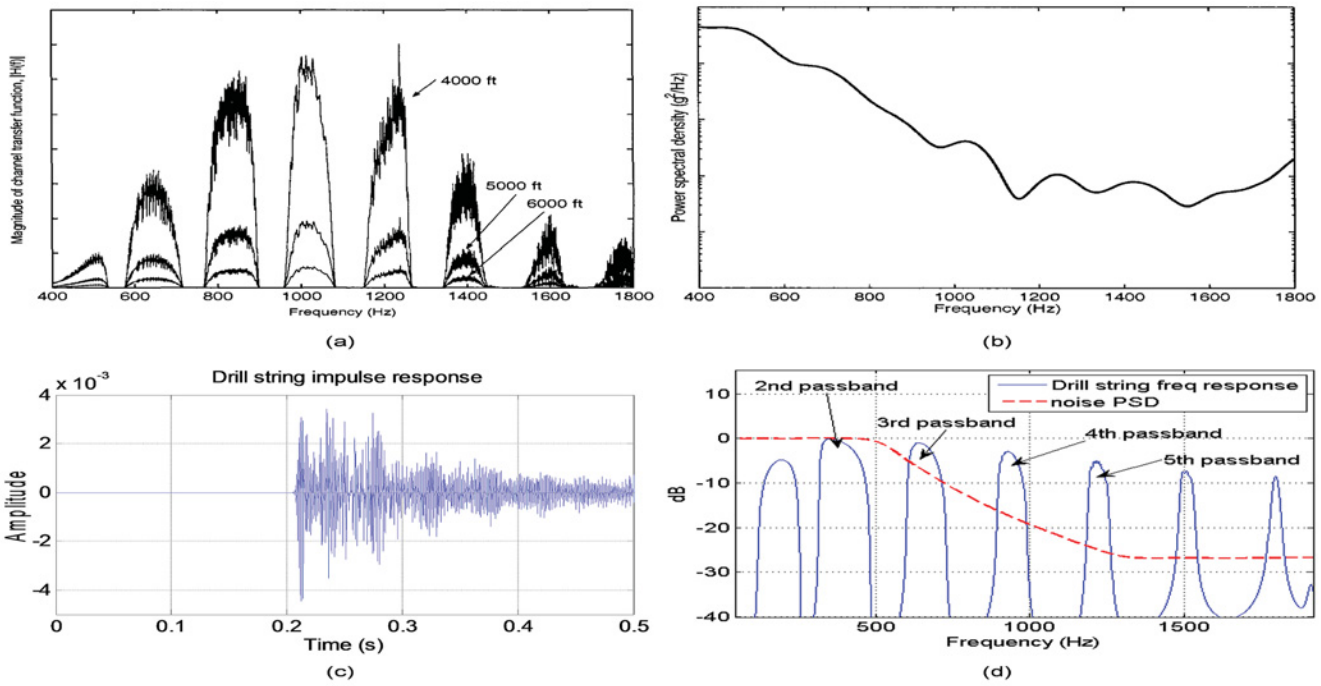

Fig. 1. (a) Drill string frequency response for various lengths (figure is taken from [6]). (b) Experimental noise PSD (figure is taken from [6]). (c) Simulated channel impulse response of 1 km steel drill string. (d) Simulated channel frequency response and noise PSD. Both plots are normalised to 0 dB.

joint-pipe length. Furthermore, the acoustic pulse experiences an attenuation in the order of 4-9 dB/1000 ft [1].

There exist two sources of noise during the drilling process: the drill bit noise and the surface noise [7]. The drill bit noise is non-stationary and depends on various factors, such as the weight on bit, type of formation, rotational speed of the bit, to name a few. The surface noise is generated by mud pumps, rotary tables and other rig operations. The drill bit noise propagates over the drill string and gets attenuated before reaching the other end but the surface noise masks the received signal directly and thus it is more significant. A typical power spectral density (PSD) of the overall drilling noise (drill bit noise plus surface noise) is shown in Figure 1(b). As can be observed from the plot, the noise PSD in non-flat and consequently the noise samples are heavily correlated in time domain. Published results have shown that the noise does not follow a Gaussian distribution; yet, the noise between the 25% and 75% percentile forms a straight line in a Q-Q plot [7]. In addition, one can notice that the noise PSD decreases by approximately 30 dB as frequency increases from 500 Hz to 1.2 kHz but remains relatively flat beyond 1.2 kHz [6]. Hence, modeling the drill string channel on the basis of the Gaussian noise assumption is a natural starting point since there is a large body of knowledge about communications in Gaussian noise channels.

Studies about the channel capacity indicate that data transmission at hundreds of bps for various drill string lengths is possible [6]. This capacity is much greater than what current state-of-art telemetry systems can achieve.

TABLE I
DRILL STRING PARAMETERS

Element	d (m)	ρ (kg/m^3)	c (m/s)	a (m^2)
Tool joint	d_2=0.4572	7870	5130	a_2=0.0129
Pipe	d_1=8.6868	7870	5130	a_1=0.0025

A. Channel modeling

The wave propagation is simulated using a finite-difference algorithm as discussed in [11]. A drill string of 110 pipes is considered. Tool joints are placed at the beginning and end of the drill string as well as between the pipes. The values for density, ρ, length of pipe, d_1, length of joint, d_2, area of pipe, a_1, area of joint, a_2 and wave speed, c, are summarized in Table I. The total length of the drill string is 1006.3 m. To measure the impulse response, a 29.67 μs excitation signal is applied from the downhole. Moreover, signal attenuation of 7 dB/1000 ft is included in the simulations. Figure 1(c) illustrates the impulse response for the duration of 0.5 s and Figure 1(d) shows the drill string frequency response. Clearly, the simulated channel behaves like a comb filter, as expected to occur in practice in the band 0-2 kHz.

Given the typical noise PSD in Figure 1(b), the drill string noise is simulated as a non-white Gaussian stochastic process. In particular, we assume that the noise samples are generated by an autoregressive-moving-average (ARMA) model of order 20. The simulated PSD is plotted in Figure 1(d) (dotted line).

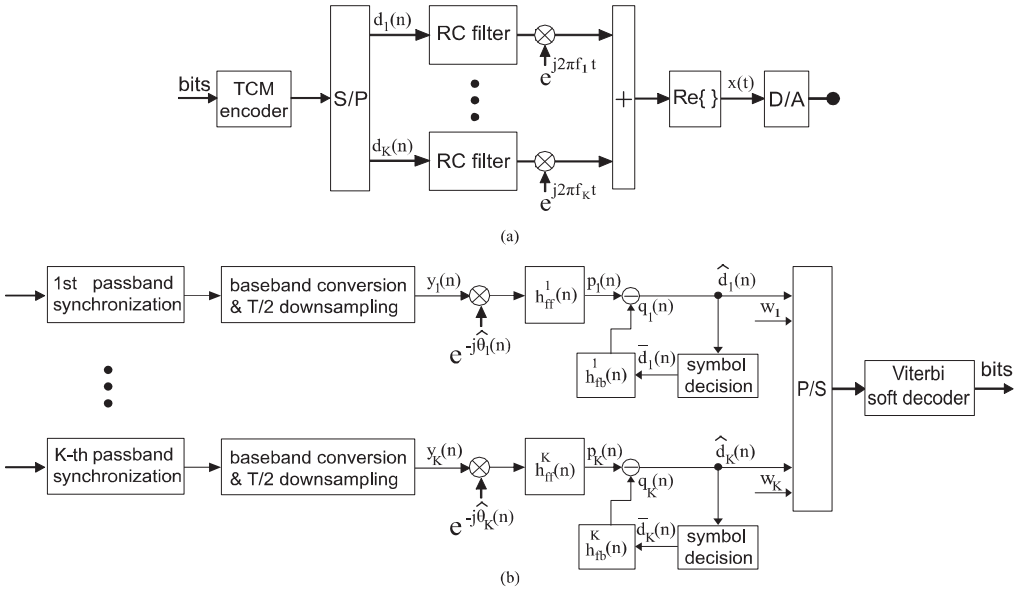

Fig. 2. Block diagram of the communications system: (a) transmitter; (b) receiver.

III. Proposed system

We now propose a multicarrier communications system for which the carriers and signal bandwidths fit within the intended passbands. The passbands locations can be identified in advance since a priori knowledge of the number of drill pipes is available. The chosen coded modulation scheme is TCM due to the channel's limited bandwidth [12]. The transmitter is shown in Figure 2(a). The incoming bit stream is encoded by a 2/3-rate, 8 state, TCM encoder with octal generators (04,02,11) to produce a coded symbol stream where each symbol is drawn from an 8-PSK signal set with average unit energy. The symbol stream is multiplexed into K substreams each of which is pulse-shaped by a raised cosine (RC) filter with signaling interval T and roll-off factor a_i. The motivation behind using the serial-to-parallel converter is to decouple bit errors coming from the same passband. The transmitted signal is given by

$$x(t) = \sum_{i=1}^{K} Re\left\{ \sum_{n} d_i(n) g(t - nT) e^{j2\pi f_i t} \right\}, \qquad (1)$$

where $\{d_i(n)\}$ are the transmitted 8-PSK symbols, $g(t)$ is the RC pulse, and f_i denotes the carrier frequency for the i^{th} passband. Note the i^{th} passband signal occupies the frequency range $f_i \pm (1+a_i)/(2T)$.

The proposed receiver is shown in Figure 2(b). The received i^{th} passband signal is coarsely synchronized after matched filtering with a known channel probe (e.g. a chirp signal), bandpass filtered and shifted to baseband. The resulting i^{th} baseband signal can be expressed as

$$y_i(t) = \sum_{n} d_i(n) h_i(t - nT - \tau_i) e^{j\theta_i(t)} + v_i(t), \qquad (2)$$

where $h_i(t)$ denotes the i^{th} baseband channel impulse response including any transmit/receive filters and piezoelectric sensors, $\theta_i(t)$ is the carrier-phase, τ_i is the signal delay within one symbol interval and $v_i(t)$ denotes the i^{th} baseband noise process.

The signal $y(t)$ is downsampled to 2 samples/symbol ($T/2$ sampling) and becomes the input of the feedforward (FF) filter of a DFE [12]. We stress that the FF filter is insensitive to exact symbol timing synchronization and becomes equivalent to the optimum linear receiver, which performs matched filtering followed by symbol-spaced equalization. At discrete time n, let the vector $\mathbf{h}_{ff}(n)$ of length N_{ff} and the vector $\mathbf{h}_{fb}(n)$ of length N_{fb} denote the feedforward filter and the feedback filter of the DFE, respectively. A $T/2$-spaced DFE coupled with carrier-phase tracking is mathematically described as follows (subscript i is omitted for brevity) [9]:

$$\begin{aligned}
e(n) &= \bar{d}(n) - \hat{d}(n) && (3)\\
\hat{d}(n) &= p(n) - q(n) && (4)\\
p(n) &= \mathbf{h}_{ff}(n)^{\dagger} \mathbf{y}(n) e^{-j\hat{\theta}(n)} && (5)\\
q(n) &= \mathbf{h}_{fb}(n)^{\dagger} \tilde{\mathbf{d}}(n) && (6)\\
\hat{\theta}(n) &= \hat{\theta}(n-1) + K_1 \Phi(n) + K_2 \sum_{i=0}^{n-1} \Phi(i) && (7)\\
\Phi(n) &= \mathrm{Im}\left\{ p(n) (\bar{d}(n) + q(n))^* \right\} && (8)\\
\mathbf{y}(n) &= [y(nT + N_1 T_s) \ldots y(nT - N_2 T_s)]^{\intercal} && (9)\\
\bar{\mathbf{d}}(n) &= [\bar{d}(n-1) \ldots \bar{d}(n - N_{fb})]^{\intercal} && (10)
\end{aligned}$$

where $\hat{d}(n)$ is the soft symbol estimate, $e(n)$ is the error signal, $p(n)$ is the output of the feedforward filter, $q(n)$ is the output of the feedback filter, $\hat{\theta}(n)$ is the carrier-phase estimate, K_1, K_2 are phase tracking parameters, $\Phi(n)$ is the phase detector output, $\mathbf{y}(n)$ is the received (baseband) signal

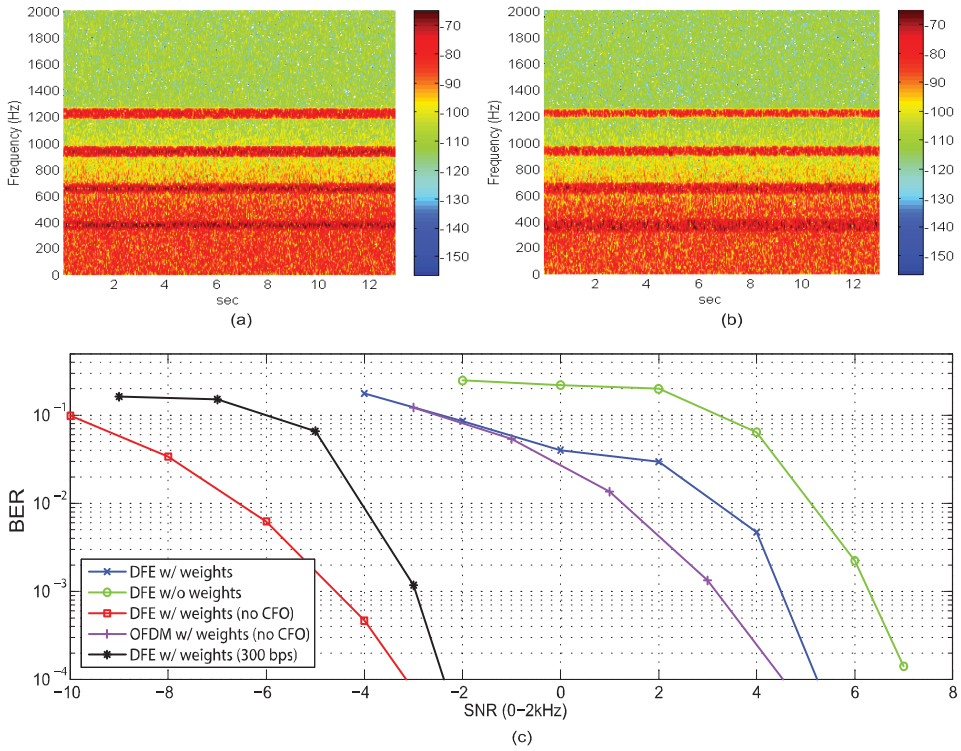

Fig. 3. (a) Spectrogram of the received multicarrier signal for 4 dB SNR. (b) Spectrogram of the received OFDM signal for 4 dB SNR. For both (a) and (b) the colorbar is in dB scale. (c) BER vs. SNR curves.

vector of length $N_{ff} = N_1+N_2+1$, $T_s = T/2$ is the sampling time of the received signal, and $\bar{\mathbf{d}}(n)$ is a vector containing the N_{fb} previously decided symbols. The DFE parameters $\mathbf{h}_{ff}(n)$ and $\mathbf{h}_{fb}(n)$ are computed recursively under the recursive least squares (RLS) algorithm such that the mean squared error (MSE), defined as $E\left[|e(n)|^2\right]$, is minimized [12].

After equalization, each soft symbol estimate $\hat{d}_i(n)$ is assigned with a positive real gain w_i. This gain reflects the reliability of each symbol based on the SNR of each passband. Although different choices of w_i exist, in this work, we make the judicious choice w_i=SNR_i, where SNR_i is the SNR of the i^{th} passband, which can be directly measured at the synchronization process. We also noticed that the impact of the SNR_i estimation error on the BER performance is insignificant. Finally, the estimated received symbols and their assigned gains are serialized and the most likely TCM codeword is determined by the Viterbi algorithm. Decoding is accomplished by minimizing the modified metric

$$\sum_{m=1}^{M} w_m \left|\hat{d}(m) - d(m)\right|^2 \qquad (11)$$

over all possible code sequences $\{d(m)\}$, where M denotes the length of the codeword in symbols. The role of w_m here is to help the decoder to emphasize on trellis paths with higher fidelity as well as to provide robustness in non-stationary noise.

IV. Simulation Results

We employ the 2nd, 3rd, 4th, and 5th passband as seen in Figure 1(a). For these passbands, the associated carrier frequencies are: $f_1 = 376\,\text{Hz}$, $f_2 = 651\,\text{Hz}$, $f_3 = 932\,\text{Hz}$, and $f_4 = 1218\,\text{Hz}$. The signaling rate is $1/T = 50$ symbols/s and the RC pulse roll-off factors for the 2nd, 3rd, 4th, and 5th passband are 0.9, 0.8, 0.2, and 0.1, respectively. Note that the information rate per passband is 2 bits/s/Hz, hence the total transmission rate is 400 bps. The transmit sampling frequency is $4\,\text{kHz}$. The drill string output is synthesized by convolving the transmit signal with the impulse response of Figure 1(c). We make the assumption that the impulse response of the drill string is constant over the duration of the communication signal. This assumption is justified by the fact that it takes about $15\,\text{min}$ to add a new pipe into the well [6]. To simulate the sampling clock mismatch between transmitter and receiver, the received signal is resampled at $4000.2\,\text{Hz}$. Then, colored Gaussian noise is added. As an example, the spectrogram of the received signal is illustrated in Figure 3(a). For each passband, the carrier-phase estimation constants are chosen as K_1=0.1 and K_2=K_1/100 and the DFE uses 28 taps (21 FF taps and 7 FB taps). The forgetting factor of the RLS algorithm is set to 0.995. Before data detection, 300 known symbols are used to train the DFE to adapt to the channel spectral characteristics.

To further elaborate on the performance of our DFE system, we compare it with a coded OFDM system. It is well known

that a properly designed coded OFDM system ensures the absence of ISI at the receiver while exploiting frequency diversity. The OFDM transmitter employs the same TCM encoder and a random symbol interleaver. The interleaver ensures decoupling of bit error coming from the same passband. Furthermore, the transmitter employs 1200 Hz bandwidth, 2048 sub-carriers and a cyclic prefix of 0.3 s. Null sub-carriers are placed at specific frequencies so that the width of each passband is almost equal to that of the mutlicarrier signal. The achieved throughput of the OFDM system is 367 bps. All data sub-carriers in the first OFDM symbol are used for channel estimation while subsequent OFDM symbols are used for data transfer. In manner similar to the mutlicarrier system, the weights, w_m, used for the Viterbi decoder are equal to the SNR of each subcarrier. It is important to note that the results regarding the OFDM system simulation assume perfect sampling synchronization and so there is no carrier-frequency offset (CFO) at the receiver. Figure 3(b) illustrates the spectrogram of the OFDM transmitted signal.

In Figure 3(c), we have plotted the BER vs. SNR curves of different systems. For all systems, the SNR is computed over the entire 0-2 kHz band. The following observations are in order:

- The effect of the reliability weights in the Viterbi decoder is clearly validated since the TCM-DFE system with weights is consistently superior than the TCM-DFE system without the weights. For instance, note the 2 dB power advantage at BER=10^{-3}. Hence, exploiting the fact that different passband experience different SNR leads to significant power savings.
- At a BER of 10^{-3}, the TCM-DFE gives about 8 dB power gain over the TCM-OFDM (assuming perfect transmitter-receiver synchronization for both systems).
- At a BER of 10^{-3}, the TCM-DFE system must pay about 10 dB power penalty as compared to the TCM-DFE with perfect synchronization. Hence, receiver synchronization should not be compromised in a real system.
- As expected, the TCM-OFDM system with perfect synchronization (no CFO) is superior to the TCM-DFE with CFO.
- When only the 3rd, 4th, and 5th passbands are employed, the effective throughput becomes 300 bps. The TCM-DFE system that employs these passbands has a power advantage of 7.5 dB over the 400 bps-TCM-DFE system. Hence, lower passbands should be avoided for better reliability.

Finally, it is instructive to check the effect of TCM coding across different passbands. Figure 4 compares the proposed TCM-DFE system (no CFO) with a DFE system based on uncoded 4-PSK signaling. Note that both systems achieve the same bit rate. Clearly, the TCM-DFE system consistently requires less SNR than the uncoded system. For instance, the 4-PSK system must pay a penalty of 7 dB SNR at BER=10^{-3}.

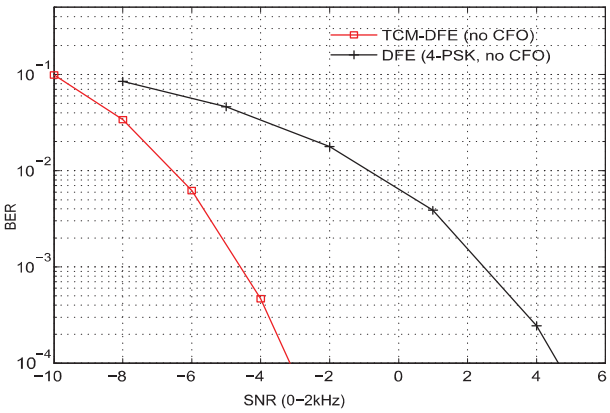

Fig. 4. Comparison of the proposed TCM-DFE system with uncoded 4-PSK DFE system.

V. Conclusion

This is the first time that an acoustic telemetry system based on equalization has been proposed for real-time LWD applications. The transmitted waveform is composed of signals of different bandwidths and carrier frequencies enabling transmission over selected passbands. Channel coding across different passbands was performed by means of a TCM encoder. To cope with ISI and imperfect sampling synchronization at each passband, the receiver performed joint carrier-phase synchronization and decision feedback equalization (DFE). In addition, the Viterbi decoder was modified to incorporate the SNR knowledge of each passband. A realistic model for the channel response of a 1-km-steel drill string was used to simulate a TCM-DFE system, capable of achieving 400 bps, roughly two orders of magnitude higher than typical mud-pulse telemetry. Furthermore, we demonstrated that this system is vastly more power efficient than its TCM-OFDM equivalent. The results of this work assumed a stationary colored Gaussian noise process; however, the true noise during drilling is expected to be non-Gaussian as well as non-stationary. Dealing with this kind of noise is a future research direction.

Acknowledgment

The authors would like to thank A. A. Muthukumaraswamy and W. Rajan from the Institute of Micro Electronics, A*STAR, Singapore, for their support.

References

[1] D. S. Drumheller, "Attenuation of sound waves in drill strings," J. Acoust. Soc. Am. vol. 94, pp., 2387-2396, 1993.
[2] V. Shah *et al*, "Design considerations for a new high data rate LWD acoustic telemetry system," in SPE Asia Pacific Oil and Gas Conference and Exhibition, pp., 1471-1477, Perth, Australia, 2004.
[3] A. K. Farraj *et al*, "Channel characterization for acoustic downhole communication systems," in SPE Annual Tech. Conf. and Exhibition, vol. 2, pp., 1206-1217, TX, United states, 2012.
[4] F. Trofimenkoff *et al*, "Characterization of em downhole-to-surface communication links," Geoscience and Remote Sensing, IEEE Transactions on, vol. 38, pp., 2539-2548, 2000.

[5] T. G. Barnes and B. R. Kirkwood, "Passbands for acoustic transmission in an idealized drill string, " J. Acoust. Soc. Am., vol. 51, pp., 1606-1608, 1972.
[6] M. Memarzadeh, "Optimal Borehole Communications Using Multicarrier Modulation," Ph.D. Thesis, Rice University, Houston, TX, USA, 2007.
[7] L. Gao *et al*, "Limits on data communication along the drillstring using acoustic waves," SPE Reservoir Evaluation & Engineering, vol. 11, no. 1, pp. 141-146, 2008.
[8] M. A. Gutierrez-Estevez et al, "Acoustic broadband communications over deep drill strings using adaptive OFDM," in IEEE Wireless Communications and Networking Conference (WCNC), pp., 4089-4094, NJ, USA, 2013.
[9] M. Stojanovic, J. A. Catipovic, and J. G. Proakis, "Phase-coherent digital communications for underwater acoustic channels", IEEE J. of Oceanic Eng. vol., 19, pp., 100-111, 1994.
[10] D. S. Drumheller, "Acoustical properties of drill strings", J. Acoust. Soc. Am., vol. 85, pp., 1048-1064, 1989.
[11] L. S. Kumar *et al*, "Optimization of Acoustic Communication for Industrial Drilling", in Proc. IEEE Conf. on Information and Comm. Technologies (ICT), pp., 18-20, 2013.
[12] J. G. Proakis, *Digital Communications*, 4th Ed., McGraw Hill, NY, 2000.